Journal of
NANOSTRUCTURES
JNS
NANOSTRUCTURES
JNS.kashanu.ac.ir

Dependence of Photocatalytic Activity of TiO_2-SiO_2 Nanopowders

Mehran Riazian*

Department of Engineering, Tonekabon branch, Islamic Azad University, Tonekabon, Iran.

Article history:
Received 14/10/2014
Accepted 8/11/2014
Published online 21/12/2014

Keywords:
Nanostructure
Photocatalytic Activity
SiO_2-TiO_2
Sol-Gel method

**Corresponding author:*
E-mail address:
m.riazian@toniau.ac.ir
Phone: 98 912 2116905
Fax: +98 192 4271105

Abstract

Structural properties and chemical composition change the photocatalytic activity in TiO_2-SiO_2 nanopowder composite. The SiO_2-TiO_2 nanostructure is synthesized based on sol–gel method. The nanoparticles are characterized by x-ray fluorescents (XRF), x-ray diffraction (XRD), tunneling electron microscopy (TEM), field emission scanning electron microscopy (FE-SEM), UV-vis. Spectrophotometer and furrier transmission create infrared absorption (FTIR) techniques. The rate constant k for the degradation of methylen blue in its aqueous solution under UV irradiation is determined as a measure of photocatalytic activity. Dependence between photocatalytic activity and SiO_2 content in the composite is determined. Rate constant k is found dependent on the content of SiO_2 in the composite that calcined at 900 oC. The addition of low composition SiO_2 to the TiO_2 matrix (lower than 45%) enhances the photocatalytic activity due to thermal stability and increasing in the surface area. The effects of chemical compositions on the surface topography and the crystallization of phases are studied.

2013 JNS All rights reserved

1. Introduction

Nanocrystalline materials are currently receiving much attention by virtue of their special chemical, physical and mechanical properties of TiO_2 nanoparticles are a function of crystal structure, nanoparticle size, morphology and the method of synthesis. TiO_2 has three naturally occurring polymorphous: anatase, rutile and brookite. Among them, the TiO_2 exists mostly inrutile and anatase phases, which both of them have the tetragonal structures. However rutile is a high-temperature stable phase and has an optical energy band gap of 3.0 eV (415 nm), anatase is formed at lower temperatures with an optical energy band gap of 3.2 eV (380 nm) and refractive index of 2.3 [1].

The size of the TiO2particles is a considerable parameter that influences physical and chemical properties of materials, so that most of the recent

researches have been focused upon the reaction of the particle size. The use and photocatalytic performance of mixed polymorphs in various applications are strongly influenced by the particle size, crystallite size, degree of crystallinity and morphology [2-4].

Among the many chemical techniques for the fabrication of materials, sol-gel processing as a moderate and adjustable method has emerged as an alternative route to control the size, morphology, structure, physical and chemical properties of inorganic oxides [5,6]. The sol-gel process is commonly applied to synthesis such TiO_2 materials owing to its several advantages such as low temperature processing and the ability to prepare materials in various shapes, compared with the conventional preparation procedures of glass and ceramics [7,8]. In this study $TiCl_4$ and TEOS used as starting materials were hydrolyzed through CH_3COOH solution.

2. Experimental procedure

In this work, TiO_2 is prepared by using hydrolysis procedure of $TiCl_4$ which is transformed to anatase by heating it at 900 ^oC. It obviously depends on the preparation procedures and TiO_2 content in combination. Anatase is generally, transformed to rutile if calcinations temperature and TiO_2 content increases.

The preparation of TiO_2-SiO_2 gel is below, such that Tetraethyl-Orthosilicate (TEOS) (Merck, $\geq 99\%$) is hydrolyzed with di-ionized water in that ethanol. Ethanol acts as a mutual solvent. TEOS in ethanol is hydrolyzed with water containing acetic acid at room temperature for 30 minutes. The solution is then mixed with titanium chloride $TiCl_4$ (Merck, $\geq 99\%$) at 0 ^oC in specific molar ratio to obtain various content of TiO_2. After 30 minutes stirring at room temperature, the sol is vibrated for 20 minutes in ultrasonic bath to deconglomerate particles and then relaxed at room temperature for 30 minutes. The sol is stirred at 60 ^oC to change into gel form and removes ethanol (about 24 hours). After creation of gelation, samples are dried at 60 ^oC to remove water and acetic acid and leaves a white to light yellow lump depends on TiO_2 content. Then the lump samples are milled with mortar and calcinated at 900 ^oC. The thermal gradient during the experimental procedure is $5^o / \min$ and the samples are put in the oven for 2 hours at calcination temperature. The procedure is shown in Fig. 1.

Table 1: Materials and corresponding molar ratio.

Materials	TEOS	$TiCl_4$	Ethanol	H_2O	CH_3COOH
Symbol	A	B	C	D	E
Molar ratio	A	B	7(A+B)	10(A+B)	2(A+B)

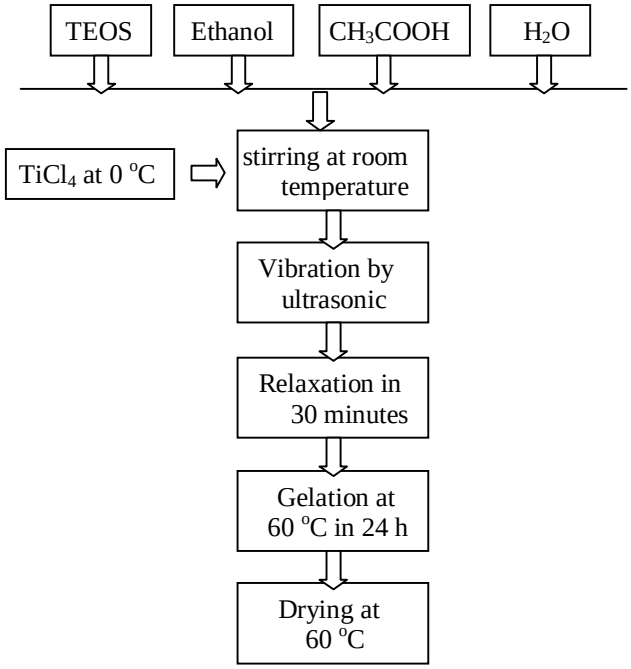

Fig. 1. The procedure for preparing TiO_2–SiO_2 in the mixture.

According to Table 1, the corresponding molar ratios of TEOS-$TiCl_4$-Ethanol-H_2O-CH_3COOH

indicate that A and B are the molar ratio of TEOS and $TiCl_4$ composition. The weight percent of ingredient in production was obtained by using XRF technique and given in Table 2.

Table 2. The result of XRF analysis.

Sample	Weight Percent
100	0.75%TiO_2-29.25%SiO_2
200	9.43%TiO_2-40.57%SiO_2
300	4.94%TiO_2-45.06%SiO_2
400	ا4.1%TiO_2-55.90%SiO_2
500	3.88%TiO_2-66.12%SiO_2
600	1.76%TiO_2-68.24%SiO_2

XRD patterns measured on a (GBC-MMA 007 (2000)) X-ray diffractometer. The diffractograms recorded with $(K_\alpha (Cu), 1.54\,Å, 0.02^o$ step size in where the speed was $10^o/\min$) radiation over a 2θ range of 10°–80°. TEM (CM10 Philips, 100 kV) used to investigate the structure and morphology of the nanoparticles. FE-SEM (S-4160 Hitachi) used to investigate the morphology of the nanoparticles. UV-visible spectrophotometer (Varian 50 scan) used to measure the methylen blue concentration. FT-IR measurements performed on a 1730 Infrared Fourier Transform Spectrometer (Perkin-Elmer) using the potassium bromide as the background.

3. Photocatalytic activity measurement

The photocatalyst degradation of methylen blue (MB)is employed as a probe to examine the photocatalytic performance of the TiO2-SiO2 nanoparticles. The photocatalytic activity experimentsare carried out at room temperature. The initial MB concentration was $100\frac{mg}{L}$. In all experiments, the photoreactor is kept at 27 ± 2 °C by using an air-conditioner. Reaction suspensions are prepared by adding 50 mg of TiO2-SiO2 nanoparticles that calcined at 900 °C as a photocatalyst into 100 ml MB aqueous solution. Prior to irradiation, the reaction mixture is sonicated (sono Swiss SW, 40 KHz) for 15 minutes and then stirred in a dark for 10 minutes to establish adsorption-desorption equilibrium. The mixture is then irradiated by UV-C light (Philips, 253.7 nm) of $33.6\frac{\mu w}{cm^2}$. Subsequently, at regular intervals of time (10,20,30,40, and 50 minutes), a portion of analytical samples is collected from the reaction suspension, centrifuged at 8000 rpm for 5 minutes and filtered through a 0.2 μm Millipore filter. Then the absorbance of the filtrate is measured using the visible spectrophotometer at 660 nm for the MB concentration. As shown in Fig. 2, the absorbance peak is around 660 nm (λmax).

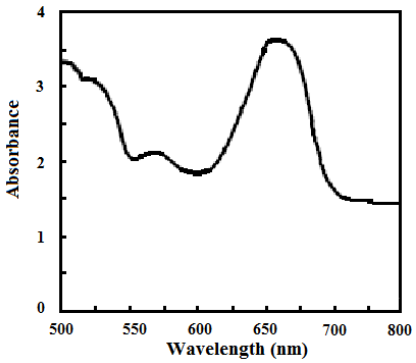

Fig. 2. UV-visible absorbance spectra and absorbance peak at 660 nm .

3. Results and discussion

Two factors determine the hydrolysis and condensation rates. The first factor is the acetic acid, which promotes the hydrolysis of TEOS; the second is the titanate formed by the chelate of acetic acid and titanium, which accelerates the condensation of TEOS [8].With respect to acetic acid, it plays two roles in the system. On the one side, it acts as the catalyst to promote the hydrolysis of TEOS; on the other side, it chelate with titanium to form titanate, which accelerates

the condensation of TEOS and retards the hydrolysis and condensation of TIOT. In the present work, the TEOS is partially hydrolyzed in methanol, water and hydrochloric acid under controlled conditions that allow the solution, i. e., sol, to yield a formable, loosely cross-linked matrix, i.e., gel.

XRD patterns of nano-TiO_2 with specific TiO_2 content in TiO_2-SiO_2 composite in rutile and anatase phasescalcined at 900 ^oC is displayed in Fig. 3. The position of all diffraction lines which corresponds to anatase and rutile phases are agreement with IUCr reference database (99-100-9974) and (99-100-4865) card, respectively. The XRD patterns of the powder samples revealthe at 25^o (101) and 48^o (200) and rutile 27^o (110), 36^o (101), 55^o (211), indicating that the samples are a mixture of anatase and rutile phases.The phase content of samples can be calculated via the integrated of anatase (101) at 25^o and rutile (110) at 27^o peaks. If the samples contain anatase and rutile phases, the mass fraction of rutile (Wr) and anatase (Wa) can be calculated through:

$$W_r = \frac{A_r}{0.886A_a+A_r}, W_a = \frac{0.886A_a}{0.886A_a+A_r} \quad (1)$$

that A_a and A_r represent the integrated intensity of the anatase (101) and rutile (110) peaks, respectively [9].

By increasing the TiO_2 content in TiO_2-SiO_2 composite up, the percent of rutile content increases (Fig. 3). This manner is due to decreasing the SiO_2 content in composite.Since the atomic radius of Si atom is smaller than Ti, the TiO_2 particle experiences a contraction and its crystal growth is retarded due to the Si atom.

The particle growth kinetics under hydrothermal conditions are determined by aggregation–recrystallization processes, allowing control over average nanoparticle size. Phase transformation of TiO_2 can be affected by SiO_2 oxides, which can improve the thermal stability of anatase, suppress particle aggregation and grain growth of anatase and increase specific area of rutile phase. The effect of the dopants demonstrates stabilizing effect on anatase since coverage of TiO_2 surface by dopant species could protect TiO_2 nanoparticles from agglomeration during calcinations temperatures. Meanwhile, incorporation of dopants into TiO_2 network might enhance straining force in anatase lattice due to structural distortion, which could further affect the growth of crystalline size in rutile phase.

Lattice strain of nanocrystallites is determined from the dependence of FWHM (Full Width Half Maximum) of diffraction lines observed in 2θ range of 10-80 on sinθ, according to the Williamson-Hall's equation [10]:

$$\beta\cos\theta = \frac{k\lambda}{L} + 4\sin\theta, \quad (2)$$

where β is FWHM observed, shape factor k is assumed to be 0.9 similar to Scherrer equation's. λ (wavelength of K_α (Cu)). The plots of βcosθ against 4sinθfor different samples are approximated to be linear. Lattice strain is determined by the slope of this linear relation. Because of lowly-crystallized powder samples, the linearity between βcosθ and 4sinθis not very evident [11]. The plots of βcosθ against 4sinθ for different diffraction lines of anatase and rutile phases are illustrated in Fig. 4 and Table 4. Experimental points for diffraction lines are scattered because the peaks are weak and broad, so that their FWHMs are difficult to be measured. As shown in Fig. 4 for the samples with 900 ^oC Calcination temperature, lattice strain increases by decreasing the TiO_2 content in composite. It can be seen in Fig. 3, lattice strain increases by increasing SiO_2 content in composite. These obtains are agreement with Inagaki results that suggests the

phase transformation from anatase to rutile structure is mainly governed by the lattice strain [11].

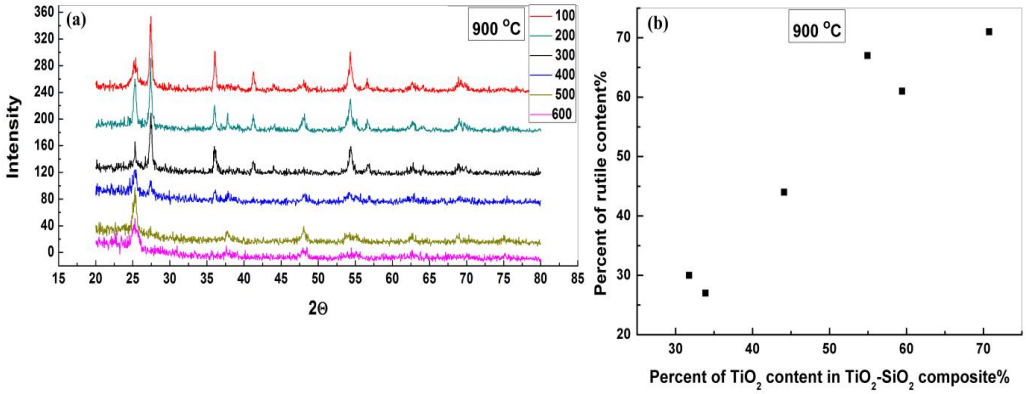

Fig. 3. (a) XRD patterns at fixed calcined temperature (900 °C) but different TiO_2 content and (b) the percent of rutile content per TiO_2 content. The inset table shows sample numbers correspond to TiO_2 content in table 2.

Table 3: The analysis of XRD patterns corresponds to Table 2. The size of grain is derived by using Scherer's equation .The phase is also extracted from database of XRD patterns (A= Anatase, R= Rutile). The angle (2θ) corresponds to more insensitive peak relevant to anatase or rutile phase.

Sample	Size (nm)	Phase (Anatase or Rotile)	Angle (2θ)
100	13	A	25.15
	33	R	27.45
200	23	A	25.30
	37	R	27.40
300	47	A	25.30
	30	R	27.45
400	13	A	25.25
	12	R	27.35
500	15	A	25.30
600	7	A	25.30

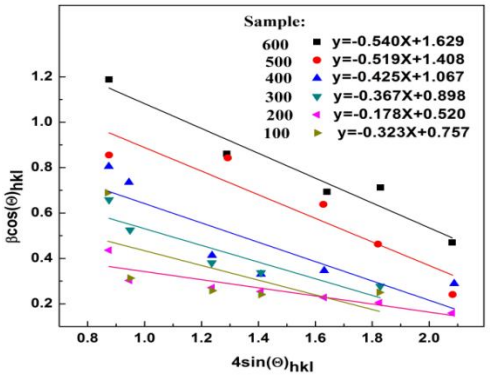

Fig. 4. Relation between βcosθ and 4sinθ (Williamson-Hall plots) with different TiO2 content in composite.

The crystallographic phases of the composite ceramic are investigated by using the XRD technique, and the results are shown in Figs. 2 and 3. As shown in this figure, different crystalline phases are formed. Fig. 2 also shows partly amorphous structure for pure sample due to the short range ordering of the network [12, 13]. The characteristics of the XRD peaks are summarized in Tables 2 and 3. The grain size values are calculated from the Scherrer equation:

$$r = \frac{0.9\lambda}{2\beta\cos\theta}, \quad (1)$$

where λ = 0.154 nm, β is the full width at half maximum (FWHM), and θ is the reflection angle. Data in Table 3 shows the influence of the reflux time on the grain size of different phases. Precursor chemistry, experimental conditions and the presence of a dopant material influence the nucleation and the growth of the different polymorphs of TiO_2 [14].

The averages of the nanocrystalline sizes are calculated based on Scherrer's formula.

Table 4. The lattice strain and rutile content obtained in different TiO2 content in composite.

Sample and content of TiO_2	**100 70.75%TiO_2-29.25%SiO_2**
Calcined Temperature °C	**900 °C**
Lattice Strain	-0.323
Percent of rutile %	71
Sample	**200 59.43%TiO_2-40.57%SiO_2**
Lattice Strain	-0.178
Percent of rutile %	62
Sample	**300 54.94%TiO_2-45.06%SiO_2**
Lattice Strain	-0.367
Percent of rutile %	75
Sample	**400 44.1%TiO_2-55.90%SiO_2**
Lattice Strain	-0.425
Percent of rutile %	44
Sample	**500 33.88%TiO_2-66.12%SiO_2**
Lattice Strain	-0.519
Percent of rutile %	26
Sample	**600 31.76%TiO_2-68.24%SiO_2**
Lattice Strain	-0.540
Percent of rutile %	30

Fig. 5 shows FE-SEM pictures of TiO_2-SiO_2 powder. This figure shows spherical and agglomerated TiO_2-SiO_2 nano-particle in samples 100 and 200. Nano-size of TiO_2-SiO_2 particles with spherical shape are observed in specific condition. Spherical shape is obvious when TiO_2 content in mixture increasesin comparison to low content TiO_2 that causes random or dendrite shape in mixed oxides. The particle size grows relatively by increasing TiO_2 content in composite. This is due to the suppressive effect of SiO_2 on the crystal growth of TiO_2. This is accordance with the result of XRD analysis, which shows that the restriction on crystal growth of TiO_2 particles.

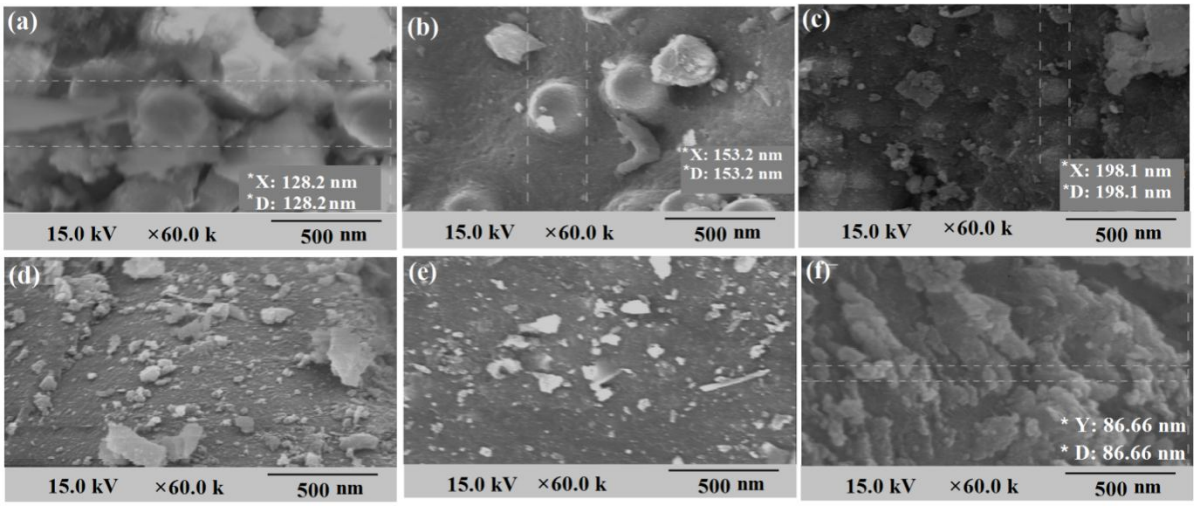

Fig.5. FE-SEM images of the powder samples with different TiO_2 content in composite, (a) sample 100, (b) sample 200, (c) sample 300, (4) sample 400, (5) sample 500, (f) sample 600.

Fig. 6 shows TEM image of the sample 100 of TiO2-SiO2 nanoparticles after calcination at 900 oC. TEM image reveals nanoparticles with an average diameter of 25 nm.

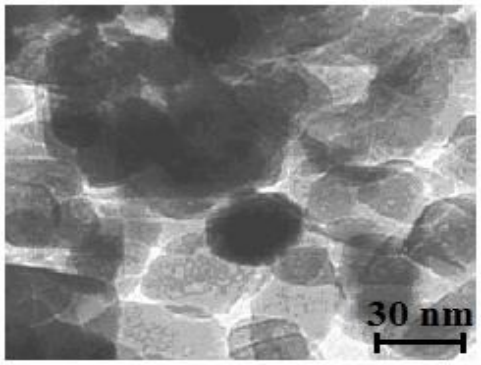

Fig. 6. TEM image of sample 100 of TiO_2-SiO_2 nanoparticles that calcined at 900 oC.

4. Photocatalytic activity of TiO_2-SiO_2

The relative concentration of MB in the solution in logarithmic scale, $Ln(\frac{C_0}{C})$ is plotted against irradiation time t of UV rays for the samples

calcined at 900 oC. The slope of the logarithmic plots is rate constant [15]. As shown in table 5, the degradation data reveals the relevant kinetic parameters, such as correlation coefficient (R2), and the degradation rate constant, k. All reactions are found to follow a linear relation, as shown in Fig. 7.

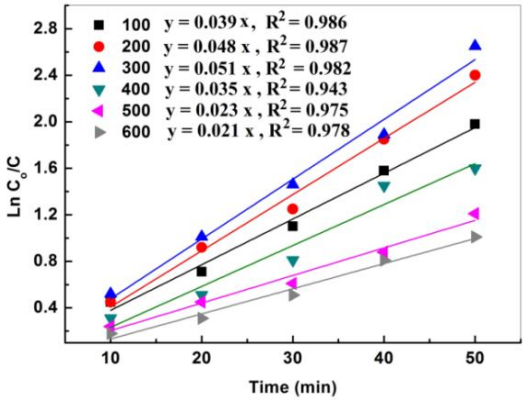

Fig. 7. The plots of relative concentration of methylen blue in logarithmic scale Ln(C_0/C) vs. irradiation time for the TiO_2-SiO_2 nanoparticles with different SiO_2 content that calcined at 900 ^oC.

As seen in Fig. 7, the photodegradation rate of MB increased as the SiO_2 content in TiO_2-SiO_2 composite made 45% and decreased with further increases in the SiO_2 content, which shows that maximum photocatalytic activity for 45% content of SiO_2 was optimum for photocatalytic degradation of MB. When TiO_2 is mixed with a suitable amount of SiO_2, the increase in photocatalytic efficiency has been attributed to improved thermal stability, the surface area and surface acidity. The increase in surface area with a reduction in particle size means an increase in the number of active sites on which the electron acceptor and donor are adsorbed and participate in the reduction-oxidation reaction.Additionally, it is reasonable that mixing TiO_2 with SiO_2 is an effective method to improve the content of surface adsorbed water and hydroxyl groups as well as the photocatalytic activity, because the phase transformation from anatase to rutile is inhibited due to the enhanced thermal stability of titania-silica mixed oxide [16,17]. The addition of high composition SiO_2 to the TiO2 matrix (more than 45%), decreases the photocatalytic activity, because the crystal growth of TiO_2 is suppressed and surface active sites are covered by inactive SiO_2.

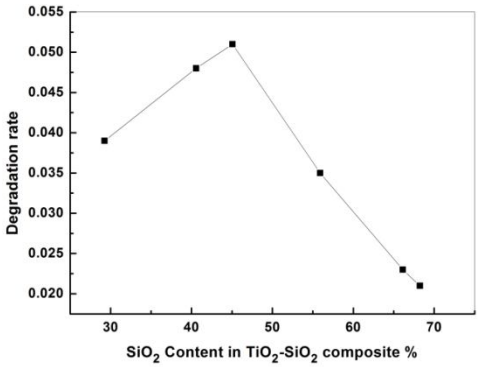

Fig. 8. Photodegradation rate of TiO_2-SiO_2 nanoparticles per SiO_2 content in composite.

Table 5. Degradation data of TiO_2-SiO_2 nanoparticles and SiO_2 content in composite.

Sample	Weight percent	k($\frac{1}{min}$)	Correlation coefficient (R^2)
100	70.75%TiO_2-29.25%SiO_2	0.039	0.986
200	59.43%TiO_2-40.57%SiO_2	0.048	0.987
300	54.94%TiO_2-45.06%SiO_2	0.051	0.982
400	44.1%TiO_2-55.90%SiO_2	0.035	0.943
500	33.88%TiO_2-66.12%SiO_2	0.023	0.975
600	31.76%TiO_2-68.24%SiO_2	0.021	0.978

The FT-IR spectrum of TiO_2-SiO_2 is shown in the Fig. 9. It consists of several bands at 1740, 1630, 1060-1220, 950, 798 and 650-740 cm^{-1}.The peaks in the spectra have been assigned according to the literature [18]. The band at 1630 and 3300 cm^{-1} are assigned to OH bending and stretching vibrations respectively. It can be ascribed to the stretching of silanol groups interacting through hydrogen bonds with water molecules. The vibration in the range 1060-1220 cm^{-1} is assignable to Si-O-Si vibration mode of isolated Si-OH

groups. The absorption band about 1070 cm^{-1} represents the characteristic bonds of Si-O-Si asymmetric stretching. The band near 950 cm^{-1} refers to Ti-O-Si asymmetric stretching. The peak near 798 cm-1 may be assigned to the O-Si-O vibration mode of SiO_2. The absorption band observed at about 950 cm^{-1} is associated with titanium in fourfold coordination with oxygen in the SiO_4^{-4} structure.Other titanium-associated absorptions occur in broad bands at 240–400 cm^{-1} and 650–730 cm^{-1}. These lie just below the host-silica absorptions at 450 and 798 cm^{-1}. In spite of the result of Y. Zhao et al. [19], this band does not appear still on the spectrum after heating treatment at 600 ◦C. The prominent IR-active bands of pure silica are ascribed to TO modes of the SiO4 network that have substantial motions of the light oxygen ions. These network modes involve vibrations of the bridging oxygen ions of corner-sharing SiO4 tetrahedra [20]. From this data, It can be concluded that titanium is in four coordination with oxygen in the SiO_4^{-4} structure, and each component in the materials is mixed on an atomic scale.

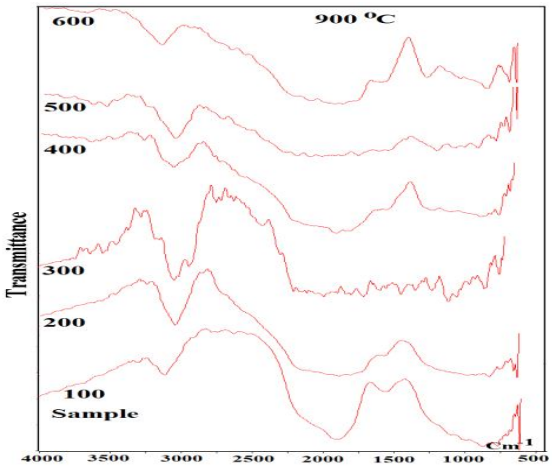

Fig. 8. FT-IR spectra of the mixed oxide at the same calcination temperatures and different TiO2 contents. The sample number labeled in figures. Are introduced in table. 3.

5. Results and discussion

We reported the synthesis of anatase and rutile nanoparticles by carefully controlling the treatment temperature of the as-prepared sample. The homogeneous hydrolysis of a metal alkoxide provided an excellent technique to prepare nanoparticle material. Experimental results indicated that the homogeneous hydrolysis of titanium chloride and Tetraethyl-Orthosilicate via sol-gel route was a promising technique for preparingmaterial with uniform nanoparticles. The effect of TiO_2-SiO_2 composite on the structural properties of powders prepared by sol-gel technique has been examined. In a two phase mixture of TiO_2 anatase transforms to rutile phase, the size of anatase and rutile nanocrystalline were shown. The mass fraction of anatase and rutile phases was calculated. It could be found that as the calcined temperature increases the percent of rutile phase content grew, as well as when the content of TiO_2 in SiO_2-TiO_2 composite increased, the percent of rutile phase content grew. Lattice strain decreased with increasing the calcination temperature, accompanying the growth of nanocrystalline size. The Scanning electron microscopy measurements showed nanostructure and morphology of powders. The TEM image revealed nanoparticles with an average diameter of 25 nm. The photodegradation rate of MB increased as the SiO_2 content in TiO_2-SiO_2 composite made 45% and decreased on further increasing in the SiO_2 content, which showed that maximum photocatalytic activity for 45% content of SiO_2 was optimum for photocatalytic degradation of MB. FTIR spectra of the composite was presented and showed the possible bonds Si-O-Ti, Ti-O-Si, Ti-O-Ti, O-Si-O and Si-O-Si.

Acknowledgment

The author thank Islamic Azad University, Tonekabon branch for financial support through a research project.

References

[1] K. Thamaphat, P. Limsuwan, B. Ngotawornchai, J. Nat. Sci. 42 (2008) 357 - 361.

[2] S. Bakardjieva, V. Stengl, L. Szatmary, J. Subrt, J. Lukac, N. Murafa, D. Niznansky, K. Cizek, J. Jirkovsky, N. Petrova, J. Mater. Chem. 12 (2006)

[3] Y. B. Khollam, S. B. Deshpande, V. Samuel and H. S. Potdar, Indian J. Engin. Mater. Sci. 15 (2008) 51-54.

[4] H. Pan, X. D. Wang, S. S. Xiao, L. G. Yu, Z. J. Zhang, Indian J. Engin. Mater. Sci. (2013) 20 561-567.

[5] M. Riazian, J. Nanostructres 3 (2013) 25-32.

[6] M. Riazian, A. Bahari, Paraman J. Phys. 78 (2012) 319–331.

[7] K Kato, A. Tsuzuki, H. Taoda, Y. Torii, T. Kato, Y. Butsugan, J. Mater. Sci. 29 (1994) 5911–5915.

[8] Y. Abe, N. Sugimoto, Y. Nagao, T. Misono, J. Non-Cryst. Solids 104 (1988) 164–169.

[9] H.Zhang, J. F. Banfdield, J. Phys. Chem. B. 104 (2000) 3481-3487.

[10] O. Carp, C. L. Huisman, A. Reller, Prog. Solid State Chem. 32 (2004) 177-178.

[11] M. Inagaki, R. Nonaka , B. Tryba, A. W Morawski, Chemosphere, 64 (2006) 437-445.

[12] J. Qiu, F. Zhuge, X. Li, X. Gao, X. Gan, L. Li, J. Mater. Chem. 22 (2012) 3549-3554.

[13] S. Sarmah, A. Kumar, Indian J. Phys. 85 (2011)713-726.

[14] S. Karan, D. D. Majumder, A Goswami, Indian J. Phys. 86 (2012) 667-762.

[15] Y. Chen, L. Lou, J. Photochem. Photobiol. A: Chemistry, 163(2004) 281-287.

[16] C. Xie, Z. Xu, Q. Yang Q, B. Xue, Y. Du, J. Zhang, Mater. Sci. Eng. B. 112 (2004) 34-41.

[17] K. Y. Jung, S. B. Park, S. Ihm, Appl. Catal. B: Environmental 51 (2004) 239-245.

[18] H. F. Yu, S. M. Wang, J. Non-Cryst. Solids 261 (2000) 260-267.

[19] Z. Yongxiang, X. Linping, W. Yongzhao, G. Chunguang, L. Diansheng Catalysis Today 93 (2004) 583–588.

[20] A. A. Gribb, J. F.Banfield, Am. Mineral 82 (1997) 717–28.